Green Chemistry

Accepted Manuscript

ROYAL SOCIETY OF CHEMISTRY

www.rsc.org/greenchem

Graphic Abstract

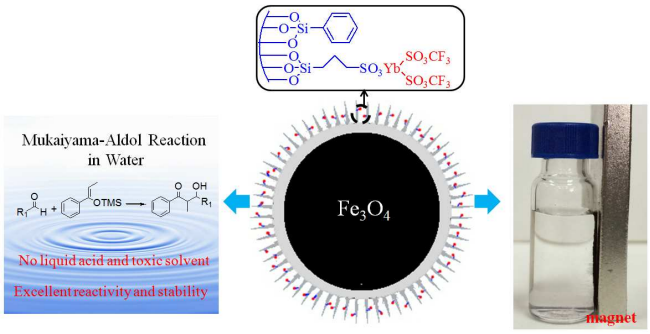

Multifunctional magnetic mesoporous silica supported $Yb(OTf)_3$ composite was demonstrated as efficient and easily recyclable catalyst for Mukaiyama-Aldol reaction in water.

Highly Active, Water-Compatible and Easily Separable Magnetic Mesoporous Lewis Acid Catalyst for Mukaiyama-Aldol Reaction in Water

Fang Zhang*, Xiaotao Wu, Chao Liang, Xiaoyan Li, Zhen Wang, Hexing Li*

The Education Ministry Key Lab of Resource Chemistry and Shanghai Key Laboratory of Rare Earth Functional Materials, Shanghai Normal University, Shanghai 200234, P. R. China

Corresponding author: zhangfang@shnu.edu.cn; HeXing-Li@shnu.edu.cn

Abstract

A novel magnetic mesoporous Lewis acid catalyst was prepared through immobilizing $Yb(OTf)_3$ on sodium propylsulphonate and phenyl groups co-functionalized magnetic core-mesoporous silica shell composite. The obtained $Yb(OTf)_2$-SO_3Na&Ph-MCMSS catalyst had a typical core-shell structure with Fe_3O_4 magnetic core, a middle amorphous silica layer and a multifunctional mesoporous silica shell with radial pore channels. In water-medium Mukaiyama-Aldol reactions, it exhibited higher catalytic reactivity than those of homogeneous catalyst $Yb(OTf)_3$, $Yb(OTf)_2$-SO_3Na-MCMSS catalysts without phenyl groups inside mesoporous channels, $Yb(OTf)_2$-SO_3Na&Ph-MCSS catalyst without mesoporous structure, $Yb(OTf)_2$-SO_3Na&Ph-MCSS mesoporous catalyst with irregular morphology and nonporous $Yb(OTf)_2$-SO_3Na-Amberlyst-15 ion-exchange resin. The systematic analysis demonstrated that this excellent catalytic performance could be attributed to the synergetic effect resulted from its radial mesoporous channel and the pore surface hydrophobicity, leading to the increased accessibility of actives sites and the decreased diffusion limitation of reactants. More importantly, this catalyst was stable in water and could be easily recycled by a simple magnet and used repetitively for at least six times.

Introduction

Homogeneous acid catalysts are mostly common used in the large-scale production of industrial chemicals and fine chemicals.[1] However, their inherent drawbacks such as the corrosivity, the environmental hazards as well as the high cost of separating the acids from the reaction system, are very difficult to meet the requirements of environmentally friendly chemical processes.[2] Moreover, some of them generally must be used under anhydrous conditions, which necessitates massive toxic, flammable organic solvents and specialized reaction vessels.[3] On the contrary, enzymes have unparalleled ability to accomplish many biological processes in aqueous medium, which inspired significant research activities in the development of solid acid catalysts for chemical synthesis in water.[4] The remarkable advantages of this catalytic system are that it could simultaneously reduce the pollution and cost resulting from liquid acids and organic solvents, coupled with the ease of recovery and recycling of homogeneous acid catalysts. Although extensive efforts have been devoted to the fabrication of solid acid catalysts, they usually displayed the inferior catalytic efficiencies in water-medium organic synthesis compared to their homogeneous compartments. The intrinsic problems in the heterogeneous catalytic systems are the decreased accessibility of actives sites and the enhanced diffusion limitation of reactants, leading to the declined catalytic reactivity and selectivity.[5] Recently, homogeneous acids immobilized on the solid matrix with high surface area or nanoscale size represented a viable solution to these circumstances because these supports could guarantee the high dispersion of active sites and the reduced mass transfer resistance.[6] However, the consequent challenge is that conventional separation methods such as filtration or centrifugation may become inefficient for these nanocatalysts.[7] To overcome this drawback, magnetically supported acid catalysts were increasingly recognized since it can be easily removed from the reaction mixture by the external magnetic separation.[8] Nevertheless, the low surface area and rapid aggregation of the typical iron oxide support are hard to maximize catalyst dispersion and activity.[9] Meanwhile, the rare functionality in the iron oxide surface limited the optimization of surface chemistry such as hydrophobicity property, resulting in unfavorable chemical microenvironment for water-medium organic reactions.[10] Therefore, one challenging strategy for the fabrication of highly active, water-

compatible and easily separable solid acid catalysts for chemical synthesis in water, is to form multifunctional nanocomposites that combine the advantages of both nanoporous support and magnetic material, which favor the high surface area, tunable chemical composition and convenient separation.

Magnetic mesoporous materials have attracted enormous interest for the development of novel heterogeneous catalysts owing to their outstanding features such as unique magnetic response, large surface area, tunable pore structure and surface functionality.[11] In the context, magnetic core-mesoporous silica shell composite (MCMSS) that comprised of a superparamagentic Fe_3O_4 core and an outer shell of ordered mesoporous silica with radial pore channels has a great potential. Owing to their distinctive advantages of both short pore channel and highly open pore structure, several different MCMSS supported catalysts containing metal nanoparticles or metal oxides have shown the remarkable enhancement of catalytic activity.[12] However, to our knowledge, Lewis acids bonded to the mesoporous channel of MCMSS support for water-medium organic synthesis has not been reported so far. Additionally, insight into the adsorption and diffusion behaviors in the confined microenvironment of MCMSS supported catalysts is rarely addressed. Herein, we reported for the first synthesis of a novel magnetic mesoporous Lewis acid catalyst ($Yb(OTf)_2$-SO_3Na&Ph-MCMSS) through immobilizing $Yb(OTf)_3$ on sodium propylsulphonate and phenyl groups co-functionalized magnetic core-mesoporous silica shell composite. Noted that it exhibited higher catalytic activity compared to $Yb(OTf)_3$ homogeneous catalyst and the control catalysts including $Yb(OTf)_2$-SO_3Na-MCMSS without phenyl groups inside mesoporous channels, $Yb(OTf)_2$-SO_3Na&Ph-MCSS without mesoporous structure, $Yb(OTf)_2$-SO_3Na&Ph-MCSS mesoporous catalyst with irregular morphology and nonporous $Yb(OTf)_2$-SO_3Na-Amberlyst-15 ion-exchange resin in water-medium Mukaiyama-Aldol reaction. This excellent catalytic performances could be attributed to the synergic effect resulted from the radially short mesoporous channel and the surface hydrophobicity, which efficiently enriched the reactants and meanwhile decreased the mass transfer limitation. Moreover, it could be easily separated using an external magnet and reused up to 6 times without loss of catalytic activity.

Experimental Section

1. Sample preparation

1. 1 Synthesis of amorphous silica coated Fe_3O_4 microspheres (SiO_2@Fe_3O_4)

Fe_3O_4 microspheres were prepared according to the method previously described by Zhao et al.[12a] In a typical run of synthesis, 0.12 g Fe_3O_4 was added into 100 ml HCl aqueous solution (0.10 M) and then the mixture was treated by ultrasonication for 30 min and washed by ethanol and water. The solid was filtrated and subsequently dispersed in the solution containing 160 ml ethanol and 30 ml deionized water. The solution was adjusted to pH 10 by 28 wt% aqueous ammonia solution. After that, 0.25 ml tetraethyl orthosilicate (TEOS) was introduced into the solution at 25^{o}C under mechanical stirring for 6.0 h. The products were collected and washed with ethanol and water, followed by drying at 60^{o}C for 12 h.

1.2 Preparation of multifunctional magnetic mesoporous silica support (SO_3Na&Ph-MCMSS)

0.20 g SiO_2@Fe_3O_4 particles were dispersed in a aqueous solution containing 0.64 g CTAB, 100 ml deionized water, 2.0 ml ammonia solution (28 wt %), and 140 ml ethanol. This mixture was ultrasonicated for 30 min and then mechanically stirred for another 30 min. Then, 0.625 ml TEOS was added dropwise to the above solution. After pre-hydrolysis for 30 min, 0.116 ml mercaptopropyltrimethoxysilane (MPTS) and 0.117 ml phenyltrimethoxysilane (PhTS) were introduced. After stirring for 12 h at 25^{o}C, the products were collected with a magnet and washed repeatedly with ethanol and deionized water. Finally, CTAB template was removed by repeated ethanol extraction under reflux condition. Next, 0.20 g solid sample was suspended into 30 ml H_2O_2 solution and stirred for 24 h. The obtained solid was washed and then added into 30 ml saturated NaCl solution for ion-exchange treatment, resulting in sodium propylsulphonate and phenyl groups co-functionalized magnetic core-mesoporous silica shell composite.

1.3 Fabrication of magnetic mesoporous Lewis acid catalyst ($Yb(OTf)_2$-SO_3Na&Ph-MCMSS)

The SO_3Na&Ph-MCMSS support was introduced into 35 ml ethanol solution containing 0.50 g $Yb(OTf)_3$ under mechanical stirring for 3.0 h at 80^{o}C. The black powder product was filtered and

washed thoroughly with absolute ethanol to eliminate un-coordinated $Yb(OTf)_3$ compound, followed by vacuum drying at 60^{o}C for 24 h.

2. Characterization

The Ytterbium loading was measured by inductively coupled plasma optical emission spectrometer (Varian VISTA-MPX). The sulfur content was determined by elemental analysis on an Element Vario EL III analyzer. Fourier transform infrared (FTIR) spectra were obtained using Thermo Nicolet Magna 550 spectrometer. X-ray powder diffraction (XRD) data were acquired on a Rigaku D/maxr B diffractometer using Cu Kα radiation. N_2 adsorption-desorption isotherms were analyzed by Quantachrome NOVA 4000e analyzer. Specific surface areas (S_{BET}) and average pore diameter (D_P) are calculated by using BET and BJH models, respectively. The morphologies were observed by transmission electron microscopy (TEM, JEM-2011). The surface electronic states were analyzed by X-ray photoelectron spectroscopy (XPS, Perkin-Elmer PHI 5000C ESCA). All the binding energy values were calibrated by using C_{1S} = 284.6 eV as a reference. The magnetic property was measured by a superconducting quantum interference device magnetometer (SQUID). The hysteresis loops of these samples were recorded at temperatures of 300 K. Water and toluene vapour absorption measurements were carried out on an intelligent gravimetric analyse (Hiden Isochema IGA-002/3) by introducing a dosed amount of high-purity vapor directly into the sample chamber and recording the weight change after stable equilibrium pressure was reached.

3. Activity Test

In a typical run of water-medium Mukaiyama-aldol reactions, a catalyst containing 0.050 mmol Yb(III), 0.5 mmol benzaldehyde, 1.0 mmol trimethyl-(1-phenylprop-1-enyloxy)silane and 3.0 ml distilled water were mixed and allowed to react at 20 °C for 16 h under mild stirring. The products were extracted with ethyl acetate, followed by analysis on a high performance liquid chromatography analyzer

(HPLC, Agilent 6410 series Triple Quad) equipped with Agilent C18 column. The reaction conversion was calculated based on benzaldehyde since trimethyl(1-phenylprop-1-enyloxy)silane was in excess.

In order to determine the catalyst recyclability, the catalyst was allowed to settle down by a magnet after each run of reactions and the clear supernatant liquid was decanted slowly. The residual solid catalyst was reused with fresh charge of water and reactant for subsequent recycle under the same reaction conditions. In all the tests, the reproducibility was checked by repeating each result at least three times and was found to be within ±5%. Meanwhile, the liquid phase of the reaction mixture was collected for ICP analysis after each reaction to test the Yb leaching.

4. Adsorption Test

To determine the adsorption performances of magnetic catalysts, 50 mg catalyst was firstly soaked in 100 ml water and oscillated at 25^{o}C for 12 h. Then, 100 ml aqueous solution including 10 ppm benzaldehyde was added into the above solution. The solution was sampled at given time intervals and the concentration of the left benzaldehyde in the solution was determined on a HPLC analyzer. The adsorption capacity was measured after reaching saturation adsorption.

Results and Discussion

The synthetic protocol of magnetic mesoporous Yb(OTf)$_2$-SO$_3$Na&Ph-MCMSS catalyst was presented in Scheme 1. We started from depositing a thin silica layer on the prefabricated Fe_3O_4 microspheres through a sol-gel coating strategy and then employed a surfactant-directed assembly approach to further generate the thiol- and phenyl-functionalized mesostructured silica/CTAB composite on the SiO_2@Fe_3O_4 surface by using cetyltrimethyl ammonium bromide (CTAB) as pore template, tetraethyl orthosilicate [TEOS, Si(OEt)$_4$], mercaptopropyltrimethoxysilane [MPTS, SH(CH$_2$)$_3$Si(OMe)$_3$] and phenyltrimethoxysilane [PTS, PhSi(OMe)$_3$] as functional precursors. After removing CTAB by

ethanol extraction, this bifunctionalized magnetic core-mesoporous silica shell composite was treated by H_2O_2 oxidation and the subsequent NaCl ion-exchange processes, resulting in the SO_3Na and Ph groups co-functionalized support (SO_3Na&Ph-MCMSS). Then, Yb(III) Lewis acids can be introduced in the mesoporous channel of the SO_3Na&Ph-MCMSS support by exposure to $Yb(OTf)_3$ solution to form the final catalyst, denoted as $Yb(OTf)_2$-SO_3Na&Ph-MCMSS. For comparison, Yb(III) Lewis acids immobilized on the SO_3Na-functionalized magnetic core-mesoporous silica shell support without hydrophobic phenyl groups inside mesoporous channel, named as $Yb(OTf)_2$-SO_3Na-MCMSS, was also synthesized by using the similar protocol. Besides, Yb(III) Lewis acids grafted on the SO_3Na- and Ph-functionalized magnetic core-silica shell support without mesoporous structure, denoted as $Yb(OTf)_2$-SO_3Na&Ph-MCSS, was also prepared through directly coordinating $Yb(OTf)_3$ with SO_3Na and Ph groups terminally bonded to SiO_2@Fe_3O_4 microspheres (Scheme S1). Meanwhile, two non-magnetic control catalysts were fabricated including $Yb(OTf)_2$-SO_3Na&Ph-MCM-41 that prepared by immobilizing $Yb(OTf)_3$ in the SO_3Na- and Ph-functionalized traditional mesoporous support MCM-41 and $Yb(OTf)_2$-SO_3Na-Amberlyst-15 catalyst that synthesized by immobilizing $Yb(OTf)_3$ on SO_3Na-functionalized commercial ion-exchange resin Amberlyst-15.

We firstly optimized the sulfur content of the functionalized support through changing the molar ratio between TEOS and MPTS silanes and obtained 1.39 mmol/g sulfur amount in the SO_3Na&Ph-MCMSS support (Table S1). Next, we investigated the immobilization conditions by using different solvents and the molar ratio between $Yb(OTf)_3$ catalyst and the SO_3Na-ligands, resulting in the optimal catalyst with 0.265 mmol/g Yb(III) loading (Table S2). The elaborated $Yb(OTf)_2$-SO_3Na&Ph-MCMSS catalyst was characterized before and after each functionalization step. FT-IR spectra (Figure 1) revealed the as-made Fe_3O_4 microspheres displayed the vibration band at 580 cm^{-1} indicative of typical Fe-O bond.[13] The SiO_2@Fe_3O_4 sample showed the new broad peaks at 1084 and 800 cm^{-1} attributed to the asymmetric stretching bonds of Si-O-Si,[14] suggesting the successful coating of a thin silica layer on the Fe_3O_4 surface. In comparison with SiO_2@Fe_3O_4 sample, $Yb(OTf)_2$-SO_3Na&Ph-MCMSS sample exhibited several addition absorption peaks. Two additional absorbance peaks around 650 and 1461 cm^{-}

[1] were indicative of the δ_{C-H} and ν_{C-C} vibrations of the phenyl groups while two additional absorbance bands around 2925 and 2855 cm^{-1} were attribute to the asymmetric and symmetric stretching modes of the C-H bond in propyl groups, revealing the co-existence of phenyl and SO_3Na moieties.[15] Meanwhile, the new peaks around 1172 cm^{-1} was ascribed to the C-F stretching absorption of CF_3 groups. In addition, the sulfate stretching vibration absorption at 1250 cm^{-1} could also be found.[16] These result clearly demonstrated the successful incorporation of $Yb(OTf)_3$ complex in the multifunctional magntic mesoporous silica support.

The chemical state of $Yb(OTf)_2$-SO_3Na&Ph-MCMSS catalyst was investigated by XPS spectrum. As shown in Figure 2, the results revealed that the $4d_{5/2}$ and $4d_{3/2}$ electronic states of all the Yb species for $Yb(OTf)_2$-SO_3Na&Ph-MCMSS catalyst were observed at 187.6 eV and 202.6 eV, suggesting that Yb element was present in a trivalence oxidation state.[17] In comparison with $Yb(OTf)_3$ sample, the binding energy of the ytterbium species in the $Yb(OTf)_2$-SO_3Na&Ph-MCMSS catalyst shifted negatively by 0.70 eV. This shift could be ascribed to the stronger electron-donating property of sulfur element in propylsulphonate groups than that in triflate ligands. This explanation could be further confirmed by XPS analysis of the sulfur element. The binding energy of the sulfur species in the $Yb(OTf)_2$-SO_3Na&Ph-MCMSS catalyst shifted positively by 0.40 eV compared to $Yb(OTf)_3$ sample. Thus, the presence of the electron transfer between $Yb(OTf)_3$ and functionalized support correlated with the observation of FT-IR spectrum, confirming that the Yb(III) Lewis acid was immobilized by replacing one triflate ligand in $Yb(OTf)_3$ with a SO_3Na ligand in the mesoporous channels of SO_3Na&Ph-MCMSS support.

We then investigated the morphological properties of the $Yb(OTf)_2$-SO_3Na&Ph-MCMSS catalyst. TEM image (Figure 3a) indicated that it had regular spherical shape with around 500 nm size. It further revealed that a typical core-shell structure of the $Yb(OTf)_2$-SO_3Na&Ph-MCMSS catalyst was formed with the magnetic core (Fe_3O_4, dark) surrounded by silica shell (SiO_2, bright). Moreover, the silica shell consisted of a middle thin silica with the thickness of ca. 15 nm and a top mesoporous silica with the thickness of about 70 nm. Notably, the HRTEM image of the $Yb(OTf)_2$-SO_3Na&Ph-MCMSS catalyst

(Figure 3b) demonstrated that the wormhole-like mesopore with the diameter of ca. 2-3 nm were observed and its pore channels were radially aligned in the top mesoporous silica shell, which resulted from the unique co-assembly of CTAB/silica on the surface of SiO_2@Fe_3O_4 microsphere.[12] The mesostructure of the Yb(OTf)$_2$-SO_3Na&Ph-MCMSS catalyst was further analyzed by using low-angle XRD analysis. It exhibited a well-resolved diffraction peak at around 2.2^o peak indicative of (100) reflection and the other two peaks at 3.8^o and 4.4^o corresponding to (110) and (200) reflections, suggesting that the hexagonal arrayed pore structure (p6mm) could be well preserved after anchoring Yb Lewis acid catalyst (Figure 4a).[18] N_2 sorption curve of the Yb(OTf)$_2$-SO_3Na&Ph-MCMSS sample (Figure 4b) exhibited a type IV isotherm with the capillary condensation step in the low pressure region and an almost constant adsorption in the high pressure region, confirming the existence of uniform mesoporous structure.[19] The narrow and sharp pore size distribution profile derived from the adsorption branch (inset) further suggested that the mesopore was uniform. And the calculated BET surface area and total pore volume were 248 m^2/g and 0.14 cm^3/g, indicating a high degree of porosity. Compared to the SO_3Na&Ph-MCMSS support (Table 1), the Yb(OTf)$_2$-SO_3Na&Ph-MCMSS sample displayed the slightly decreased value of S_{BET}, V_P and D_P due to the presence of the bulky Lewis acid moieties inside the mesoporous channels.

Mukaiyama-Aldol reaction is an important carbon-carbon bond formation process that has the ability to obtain β-hydroxycarbonyl compounds in a regio-, stereo-, and enantioselective manner.[20] To investigate the utility of our novel Yb(OTf)$_2$-SO_3Na&Ph-MCMSS catalyst, water-medium Mukaiyama-Aldol reaction involved with benzaldehyde and trimethyl-(1-phenylprop-1-enyloxy)silane was firstly carried out under the procedure described in the experimental section. Firstly, the control experiments indicated that the blank experiments with SiO_2@Fe_3O_4 and SH&Ph-MCMSS samples could not give any products in water-medium Mukaiyama-Aldol reaction, indicating Yb^{3+} Lewis acid were the really active species (Table S3). Furthermore, the preliminary experiments demonstrated that the optimum reaction temperature was 20^{o}C (Figure S1). By adjusting the catalyst amount in the reaction system, the total Yb(III) amount in each reaction was fixed with 0.05 mmol loading (Figure S2). Under this optimal

reaction conditions, $Yb(OTf)_2$-SO_3Na&Ph-MCMSS catalyst proceeded rapidly and cleanly to the coupling product with 97.2% yield after 16 h (Figure 5). Interestingly, homogeneous $Yb(OTf)_3$ catalyst displayed the significant decreased catalytic efficiency with 72.4% yield in the same conditions. The different catalytic reactivities of $Yb(OTf)_2$-SO_3Na&Ph-MCMSS and $Yb(OTf)_3$ catalysts could be interpreted based on the reaction mechanism. The carbonyl groups in benzaldehyde firstly interacted with Yb(III) Lewis acid through σ bonding coordination and trimethyl(1-phenylprop-1-enyloxy)silane attacked the activated benzaldehyde to generate the final aldol product. Owing to the low solubility of two reactants in water, the diffusion and adsorption of reactants played a critical role in determining the yield. Therefore, the excellent catalytic reactivity of $Yb(OTf)_2$-SO_3Na&Ph-MCMSS catalyst could be attributed to the strong surface hydrophobicity derived from the location of phenyl groups in the mesoporous channels. Accordingly, we used the control $Yb(OTf)_2$-SO_3Na-MCMSS catalyst without phenyl groups inside the mesoporous channels to confirm the merit of hydrophobic surface.[21] As expected, it exhibited the remarkable declined catalytic activity with 56.2% yield. To further validate the enhanced hydrophobicity of $Yb(OTf)_2$-SO_3Na&Ph-MCMSS catalyst, both water and toluene absorption experiments were tested (Figure 6). All the isotherms were of type V indicative of weak absorbent-absorbate interaction.[22] However, $Yb(OTf)_2$-SO_3Na&Ph-MCMSS sample had a higher affinity for toluene than that of $Yb(OTf)_2$-SO_3Na-MCMSS sample, indicating that it was more hydrophobic. Meanwhile, the adsorption capacity of $Yb(OTf)_2$-SO_3Na&Ph-MCMSS for toluene (24.2 wt.%) was much higher than that of water (2.41 wt.%). On the contrary, $Yb(OTf)_2$-SO_3Na-MCMSS showed the higher adsorption capacity (16.4 wt.%) of water than that of toluene (4.59 wt.%) and water. These results demonstrated that $Yb(OTf)_2$-SO_3Na-MCMSS was selective adsorption for hydrophobic organic substance.

Moreover, $Yb(OTf)_2$-SO_3Na&Ph-MCMSS catalyst was more active than the other control $Yb(OTf)_2$-SO_3Na&Ph-MCSS catalyst with 69.5% yield in the same reaction. Firstly, it had the similar chemical microenvironment with that of the $Yb(OTf)_2$-SO_3Na&Ph-MCMSS catalyst due to the same $Yb(OTf)_3$ immobilization approach (Experimental section in Supporting Information). Moreover, we

also calculated the density of Yb(III) active sites in the supports for these two catalysts. Moreover, the C_{Yb}/S_{BET} value that calculated from the Yb content and the specific surface area of the $Yb(OTf)_2$-SO_3Na&Ph-MCSS and $Yb(OTf)_2$-SO_3Na&Ph-MCSS catalysts was $1.07x10^{-3}$ and $1.02x10^{-3}$ mmol/m^2, respectively. The approximate data confirmed almost the identical active site density. Furthermore, we considered the diffusion distance for the reactants since the longer reaction distance decreased the molecule interaction and thus led to the lower catalytic activity.[23] However, TEM image (Figure 7) revealed that the $Yb(OTf)_2$-SO_3Na&Ph-MCSS catalyst was presented in uniform spheres with the diameter of about 440 nm. Meanwhile, it displayed the core-shell structure with a magnetic core and a thin silica shell with around 30 nm thickness, demonstrating the reaction should be happened in the catalyst surface without significant diffusion resistance. Therefore, the higher catalytic efficiency of the $Yb(OTf)_2$-SO_3Na&Ph-MCSS catalyst could be mainly attributed to the existed mesoporous structure with radial pore alignment, in which unique confined environment concentrated the reactants and thus led to the enhanced activity.[24] In order to prove the above hypothesis, benzaldehyde adsorption test in water over $Yb(OTf)_2$-SO_3Na&Ph-MCMSS and $Yb(OTf)_2$-SO_3Na&Ph-MCSS catalysts were measured. As shown in Figure 8a, $Yb(OTf)_2$-SO_3Na&Ph-MCMSS catalyst displayed higher saturated adsorption capacity (65.0%) than $Yb(OTf)_2$-SO_3Na&Ph-MCSS catalyst (42.3%). Thus, we concluded that the higher enrichment capacity of the organic reactants promoted the catalytic reactivity of the $Yb(OTf)_2$-SO_3Na&Ph-MCMSS catalyst in water-medium organic reactions.

In addition, we also compared the catalytic performance of $Yb(OTf)_2$-SO_3Na-MCMSS catalyst with two non-magnetic catalysts including SO_3Na- and Ph-functionalized MCM-41 supported $Yb(OTf)_3$ catalyst ($Yb(OTf)_2$-SO_3Na&Ph-MCM-41) and conventional ion-exchange resin supported $Yb(OTf)_3$ catalyst ($Yb(OTf)_2$-SO_3Na-Amberlyst-15). XRD pattern, N_2 sorption isotherm and TEM picture of $Yb(OTf)_2$-SO_3Na&Ph-MCM-41 demonstrated its two-dimensional hexagonal ordered mesoporous structure. However, SEM images revealed that it displayed an irregular morphology with a very broad particle size distribution (Figure S3). SEM image and TEM picture of $Yb(OTf)_2$-SO_3Na-Amberlyst-15 catalyst showed that it was nonporous solid (Figure S4). In the same reaction conditions

(Table S3), $Yb(OTf)_2$-SO_3Na&Ph-MCM-41 obtained the relative high yield of 87.3% while $Yb(OTf)_2$-SO_3Na-Amberlyst-15 got the yield of 75.4%. The inferior catalytic efficiency for $Yb(OTf)_2$-SO_3Na&Ph-MCM-41 could be attributed to its increased diffusion resistance while the low surface area of $Yb(OTf)_2$-SO_3Na-Amberlyst-15 caused the decreased catalytic activity (Table 1), furthermore demonstrating the advantage of $Yb(OTf)_2$-SO_3Na-MCMSS catalyst.

Encouraged by these results, we examined the scope of $Yb(OTf)_2$-SO_3Na&Ph-MCSS catalyzed Mukaiyama-Aldol coupling on a series of substances. Similarly, 4-substituted benzaldehyde derivates having either the electron-accepting group (NO_2-) or the electron-donating group (CH_3O-) also led to high yields of coupling products. Notably, 2-naphthaldehyde with large molecular size also could be converted to product with excellent yield around 90%. Next, we investigated the conversion of aliphatic aldehydes with trimethyl(1-phenylprop-1-enyloxy)silane, especially for water-soluble aldehyde such as formaldehyde. As shown in Table 2, the good yields were observed for all the aliphatic aldehydes. In the same way, $Yb(OTf)_2$-SO_3Na&Ph-MCSS catalyst exhibited higher catalytic activity and selectivity than those of $Yb(OTf)_2$-SO_3Na-MCMSS and $Yb(OTf)_2$-SO_3Na&Ph-MCSS catalysts for all the reactants, demonstrating its universal advantage in the water-medium Mukaiyama-Aldol reaction.

To determine whether the heterogeneous or the dissolved homogeneous Yb(III) compound was the real acid active species, the following procedure that proposed by Sheldon group was carried out.[25] After reacting for 8.0 h that the conversion exceeded 50% in Mukaiyama-Aldol reaction between benzaldehyde and trimethyl-(1-phenylprop-1-enyloxy)silane, the mixture was separated by an external magnet to remove the solid catalyst and then allowed the mother liquor to react for another 10 h under the same reaction conditions. No significant change in the benzaldehyde conversion was observed, suggesting that the catalytic reactivity by the leaching Yb(III) catalyst could be approximately excluded in the present reaction. Moreover, the liquid phase of the reaction mixture was collected after each reaction. ICP-AES analysis confirmed very low amount of Yb (less than 2.0 ppm) in the reaction mixture. Even if a long time reaction (36 h) was carried out or a large amount of the catalyst (0.50 g) was added, a low Yb leaching amount (less than 3.5 ppm) was detected after reaction for both cases.

Therefore, the present catalysis indeed was heterogeneous in nature rather than any dissolved acid species leached from the $Yb(OTf)_2$-SO_3Na&Ph-MCSS catalyst.

An attractive advantage of $Yb(OTf)_2$-SO_3Na&Ph-MCSS catalyst was its easy separation using external magnet, which drastically reduce the operating time and cost arose from the separation of products from a reaction mixture. The reusability of magnetic mesoporous catalysts relied on their magnetic-response property since the external coating on Fe_3O_4 surface usually decreased their magnetic responsivity.[26] Wide-angle XRD pattern of exhibited well resolved diffraction peaks for the Pd-PPh_2-MCMS catalyst (Figure 9a). All the peaks can be exactly indexed to the diffractions of Fe_3O_4 crystal in cubic spinel structure, suggesting the coating process and surface modification have no effect on the crystalline properties of magnetite. We furthermore analyzed its magnetic behaviors using a magnetometer at 300 K (Figure 9b). The result indicated that $Yb(OTf)_2$-SO_3Na&Ph-MCSS catalyst had magnetization saturation value of 21.3 emu/g, demonstrating its superparamagnetic behavior.[27] Thus, it could simply be recovered in a short time (< 10 s) by fixing a magnet near to the reaction vessel (Figure 9c-d). Figure 10 showed the recyclability of the $Yb(OTf)_2$-SO_3Na&Ph-MCSS catalyst during water-medium Mukaiyama-Aldol reaction between benzaldehyde and trimethyl-(1-phenylprop-1-enyloxy)silane. No remarkable decrease could be found in the catalytic activity after being used repetitively six times, revealing its superiority over the corresponding $Yb(OTf)_3$ homogeneous catalyst for reducing cost and diminishing environmental pollution from homogeneous acid and organic solvents. The ICP analysis confirmed that only about 4.8% of the Yb species leached off after six cycles in the recycled $Yb(OTf)_2$-SO_3Na&Ph-MCSS catalyst, demonstrating that the existence of mesoporous structure could effectively restrict the active sites leaching.[28] In addition, N_2 sorption isotherm and low-angle XRD pattern (Figure S5) confirmed that ordered 2-D mesostructure and high surface area were also well preserved. Moreover, TEM image (Figure S6) of the recycled $Yb(OTf)_2$-SO_3Na&Ph-MCMSS catalyst after six repetitions indicated that it could retain the spherical morphology and mesoporous structure and only partial particle aggregation existed, suggesting the relatively high structure stability in water-medium organic synthesis.

Conclusion

In summary, we have developed a novel approach to prepare highly active and water-compatible magnetic mesoporous Lewis acid catalyst ($Yb(OTf)_2$-SO_3Na&Ph-MCMSS) by introducing $Yb(OTf)_3$ into the mesoporous channel of SO_3Na- and Ph-functionalized magnetic core-silica shell support. Notably, it displayed a remarkable enhancement in the catalytic activity for water-medium Mukaiyama-Aldol reaction compared to $Yb(OTf)_3$ homogeneous catalyst. In comparison with that bonded to magnetic core-silica shell catalyst without mesoporous structure, SO_3Na-functionalized magnetic core-silica shell support without phenyl groups inside the mesoporous channel, SO_3Na- and Ph-functionalized mesoporous support with irregular morphology and nonporous SO_3Na-functionalized conventional ion-exchange resin support, it also exhibited the higher catalytic reactivity and selectivity. Control experiments and systematic characterizations confirmed that its unique mesoporous confinement effect and surface hydrophobicity could enrich the reactants and simultaneously reduce the diffusion transfer limitation in water, resulting in the enhanced catalytic efficiency. Moreover, it could be easily recycled by using an external magnet and reused at least six times without loss of catalytic activity. This work provides the novel synthetic approach towards the preparation of highly efficient and easily recycled heterogeneous catalysts for more environmental friendly chemical transformations.

Acknowledgements

This work was supported by the Natural Science Foundation of China (21107071 and 51273112), PCSIRT (IRT1269) and Shanghai Government (13QA1402800 and 12CG52).

Notes and references

[1] J. A. Melero, R. van Grieken, G. Morales, *Chem. Rev.* 2006, **106**, 3790-3812.

[2] T. M. Jyothi, M. L. Kaliya, M. V. Landau, *Angew. Chem. Int. Ed.* 2001, **40**, 2881-2884.

[3] A. Corma, H. García, *Chem. Rev.* 2003, **103**, 4307-4365.

[4] R. N. Butler, A. G. Coyne, *Chem. Rev.* 2010, **110**, 6302-6337.

[5] K. Inumaru, T. Ishiharam, Y. Kamiya, T. Okuhara, S. Yamanaka, *Angew. Chem. Int. Ed.* 2007, **46**, 7625-7628.

[6] F. D. Clippel, M. Dusselier, S. V. D. Vyver, L. Peng, P. Jacobs, B. F. Sels, *Green Chem.* 2013, **15**, 1398-1430.

[7] J. P. Ge, T. Huynh, Y. X. Hu, Y. D. Yin, *Nano Lett.* 2008, **8**, 931-934.

[8] (a) V. Polshettiwar, R. Luque, A. Fihri, H. B. Zhu, M. Bouhrara, J. M. Basset, *Chem. Rev.* 2011, **111**, 3036-3075; (b) S. Shylesh, V. Schünemann, W. R. Thiel, *Angew. Chem. Int. Ed.* 2010, 49, 3428-3459; (c) M. B. Gawande, P. S. Brance, R. S. Varma, *Chem. Soc. Rev.* 2013, **42**, 3371-3393.

[9] M. Feyen, C. Weidenthaler, F. Schüth, A. H. Lu, *Chem. Mater.* 2010, **22**, 2955-2961.

[10] F. C. Zheng, Q. W. Chen, L. Hu, N. Yan, X. K. Kong, *Dalton Trans.* 2014, **43**, 1220-1227.

[11] (a) J. Liu, S. Z. Qiao, Q. H. Hu, G. Q. Lu, *Small* 2011, **7**, 425-443; (b) J. P. Ge, Q. Zhang, T. R. Zhang, Y. D. Yin, *Angew. Chem. Int. Ed.* 2008, **47**, 8924-8928; (c) A. H. Lu, W. Schmidt, N. Matoussevitch, H. Boennemann, B. Spliethoff, B. Tesche, E. Bill, W. Kiefer, F. Schüeth, *Angew. Chem. Int. Ed.* 2004, **43**, 4303-4306; (d) D. Damodara, R. Arundhathiab, P. R. Likhar, *Catal. Sci. Technol.* 2013, **3**, 797-802; (e) H. Q. Yang, Y. W. Wang, Y. Qin, Y. Z. Chong, Q. Z. Yang, G. Li, L. Zhang, W. Li, *Green Chem.* 2011, **13**, 1352-1361; (f) R. B. Nasir Baig, R. S. Varma, *Green Chem.* 2013, **15**, 398-417; (g) Z. M Cui, Z. Chen, C. Y. Cao, L. Jiang, W. G. Song, *Chem. Commun.* 2013, **49**, 2332-2334; (h) J. H. Yang, D. F. Wang, W. D. Liu, X. Zhang, F. L. Bian, W. Yu, *Green Chem.* 2013, **15**, 3429-3437; (i) H. R. Shaterian, M. Aghakhanizadeh, *Catal. Sci. Technol.* 2013, **3**, 425-428.

[12] (a) Y. H. Deng, Y. Cai, Z. K. Sun, J. Liu, C. Liu, J. Wei, W. Li, C. Liu, Y. Wang, D. Y. Zhao, *J. Am. Chem. Soc.* 2010, **132**, 8466-8473; (b) S. Okada, S. Ikurumi, T. Kamegawa, K. Mori, H. Yamashita, *J. Phys. Chem. C* 2012, **116**, 14360-14367; (c) Y. Chi, Q. Yuan, Y. J. Li, L. Zhao, N. Li, X. T. Li, W. F. Yan, *J. Hazard. Mater.* 2013, **262**, 404-411; (d) P. Li, Y. Yu, H. Liu, C. Y. Cao, W. G. Song, *Nanoscale* 2014, **6**, 442-448.

[13] S. Shylesh, L. Wang, S. Demeshko, W. R. Thiel, *ChemCatChem* 2010, **2**, 1543-1547.

[14] C. S. Gill, B. A. Price, C. W. Jones, *J. Catal.* 2007, **251**, 145-152.

[15] Q. H. Yang, M. P. Kapoor, S. Inagaki, *J. Am. Chem. Soc.* 2002, **124**, 9694-9695.

[16] R. Kumar, J. P. Sharma, S. S. Sekhon, *Eur. Polym. J.* 2005, **41**, 2718-2725.

[17] S. Suga, S. Ogawa, H. Namatame, M. Taniguchi, A. Kakizaki, T. Ishii, A. Fujimori, S. J. Oh, T. Miyahara, A. Ochiai, T. Suzuki, T. Kasuya, *J. Phys. Soc. Jpn.* 1989, **58**, 4534-4543.

[18] D. Y. Zhao, J. L. Feng, Q. S. Huo, N. Melosh, G. H. Fredrickson, B. F. Chmelka, G. D. Stucky, *Science* 1998, **279**, 548-552.

[19] K. Nakajima, I. Tomita, M. Hara, S. Hayashi, K. Domen, J. N. Kondo, *Adv. Mater.* 2005, **17**, 1839-1842.

[20] S. B. Jennifer Kan, K. K. H. Ng, I. Paterson, *Angew. Chem. Int. Ed.* 2013, **52**, 9097-9108.

[21] R. Siegel, E. Domingues, R. De Sousa, F. Jérôme, C. M. Morais, N. Bion, P. Ferreira, L. Mafra, *J. Mater. Chem.* 2012, **22**, 7412-7419.

[22] F. Zhang, J. Yin, W. Chai, H. X. Li, *ChemSusChem* 2010, **3**, 724-727.

[23] W. H. He, F. Zhang, H. X. Li, *Chem. Sci.* 2011, **2**, 961-966.

[24] M. Sanlés-Sobrido, M. Pérez-Lorenzo, B. Rodríguez-González, V. Salgueiriño, M. A. Correa-Duarte, *Angew. Chem. Int. Ed.* 2013, **51**, 3877-3882.

[25] R. A. Sheldon, M. I. Wallau, W. C. E. Arends, U. Schuchardt, *Acc. Chem. Res.* 1998, **31**, 485-493.

[26] M. Shokouhimehr, Y. Piao, J. Kim, Y. Jang, T. Hyeon, *Angew. Chem. Int. Ed.* 2007, **46**, 7039-7043.

[27] M. J. Jin, D. H. Lee, *Angew. Chem. Int. Ed.* 2010, **49**, 1119-1022.

[28] P. Sreekanth, S. Kim, T. Hyeon, B. Kim, *Adv. Synth. Catal.* **2003**, **345**, 936-938.

Table 1 Chemical composition and physical parameter of different Yb catalysts.

Sample	S content (mmol/g)	Yb loading (mmol/g)	S_{BET} (m^2/g)	Vp (cm^3/g)	Dp (nm)
SO_3Na&Ph-MCMSS	1.39	/	289	0.21	2.5
Yb(OTf)$_2$-SO_3Na&Ph-MCMSS	1.39	0.265	248	0.14	2.2
Yb(OTf)$_2$-SO_3Na-MCSS	1.41	0.270	265	0.17	2.3
Yb(OTf)$_2$-SO_3Na&Ph-MCSS	0.20	0.0370	36	0.02	1.2
Yb(OTf)$_2$-SO_3Na&Ph-MCM-41	1.80	0.385	515	0.55	2.5
Yb(OTf)$_2$-SO_3Na-Amberlyst-15	0.17	0.0320	40	/	/

Table 2 Catalytic performances of different Yb catalysts in water-medium Mukaiyama-Aldol reaction.[a]

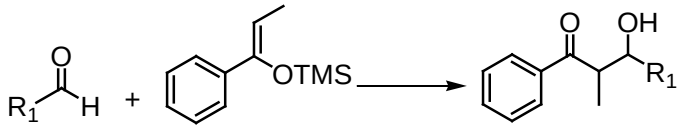

Catalyst	R_1	Conversion (%)	Selctivity (%)	Yield (%)
$Yb(OTf)_2$-SO_3Na&Ph-MCMSS	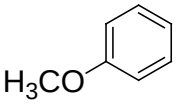	92.5	99	92.4
$Yb(OTf)_2$-SO_3Na-MCSS		53.6	99	53.5
$Yb(OTf)_2$-SO_3Na&Ph-MCSS		64.3	99	64.2
$Yb(OTf)_2$-SO_3Na&Ph-MCMSS	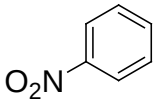	95.5	99	95.4
$Yb(OTf)_2$-SO_3Na-MCSS		62.3	99	62.2
$Yb(OTf)_2$-SO_3Na&Ph-MCSS		68.6	99	68.5
$Yb(OTf)_2$-SO_3Na&Ph-MCMSS	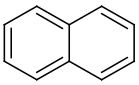	90.0	99	89.9
$Yb(OTf)_2$-SO_3Na-MCSS		47.8	99	47.7
$Yb(OTf)_2$-SO_3Na&Ph-MCSS		62.1	99	62.0
$Yb(OTf)_2$-SO_3Na&Ph-MCMSS		95.2	99	95.1
$Yb(OTf)_2$-SO_3Na-MCSS	C_5H_{11}[b]	59.2	99	59.1
$Yb(OTf)_2$-SO_3Na&Ph-MCSS		71.0	99	70.9
$Yb(OTf)_2$-SO_3Na&Ph-MCMSS		92.1	84[c]	77.3
$Yb(OTf)_2$-SO_3Na-MCSS	H[b]	75.9	56	42.5
$Yb(OTf)_2$-SO_3Na&Ph-MCSS		83.5	68	56.8

[a]Reaction conditions: 0.50 mmol benzaldehyde, 1.0 mmol silane, 0.050 mmol Yb, 3.0 ml water, 20°C, 16 h. [b] 10 mmol HCHO in 37% aqueous solution, 1.0 mmol silane. [c] The selectivity was was determined based on its ratio to the byproduct propiophenone from hydrolysis of silane.

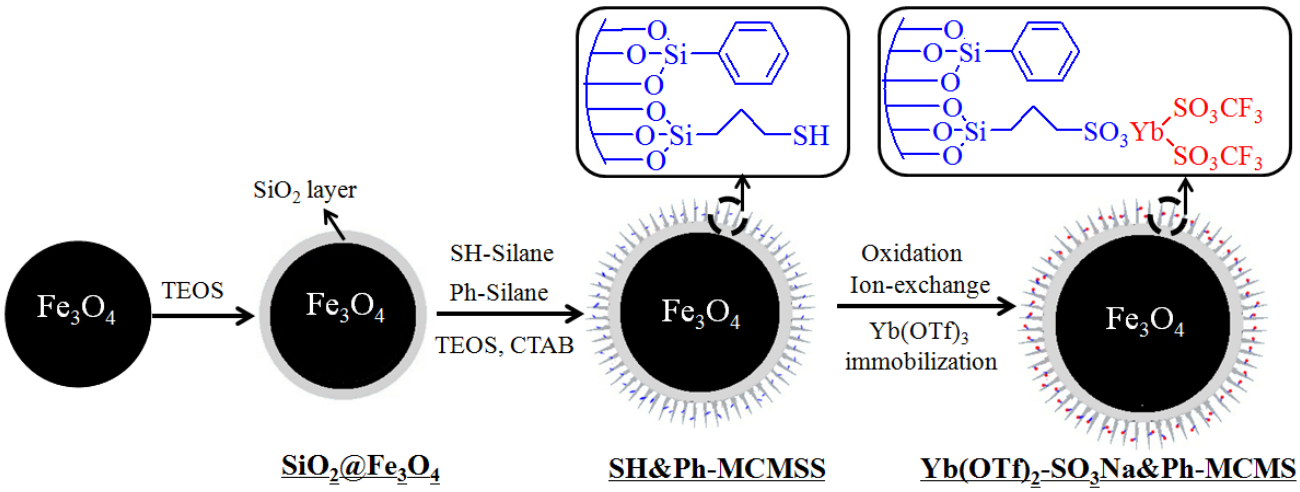

Scheme 1 Schematic illustration of the synthesis of magnetic mesoporous $Yb(OTf)_2$-SO_3Na&Ph-MCMSS catalyst.

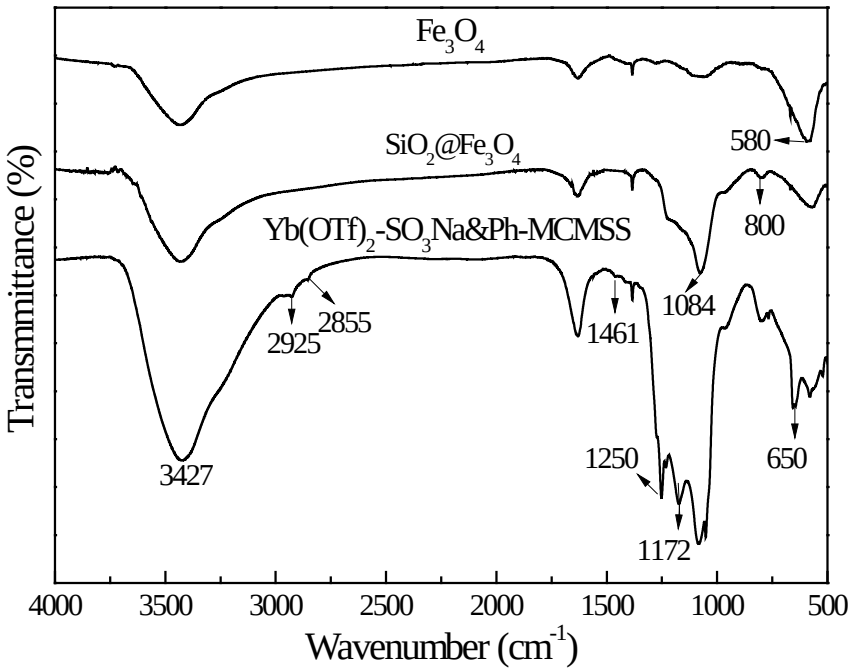

Figure 1 FTIR spectra of Fe_3O_4, SiO_2@ Fe_3O_4 and Yb(OTf)$_2$-SO_3Na&Ph-MCMSS samples

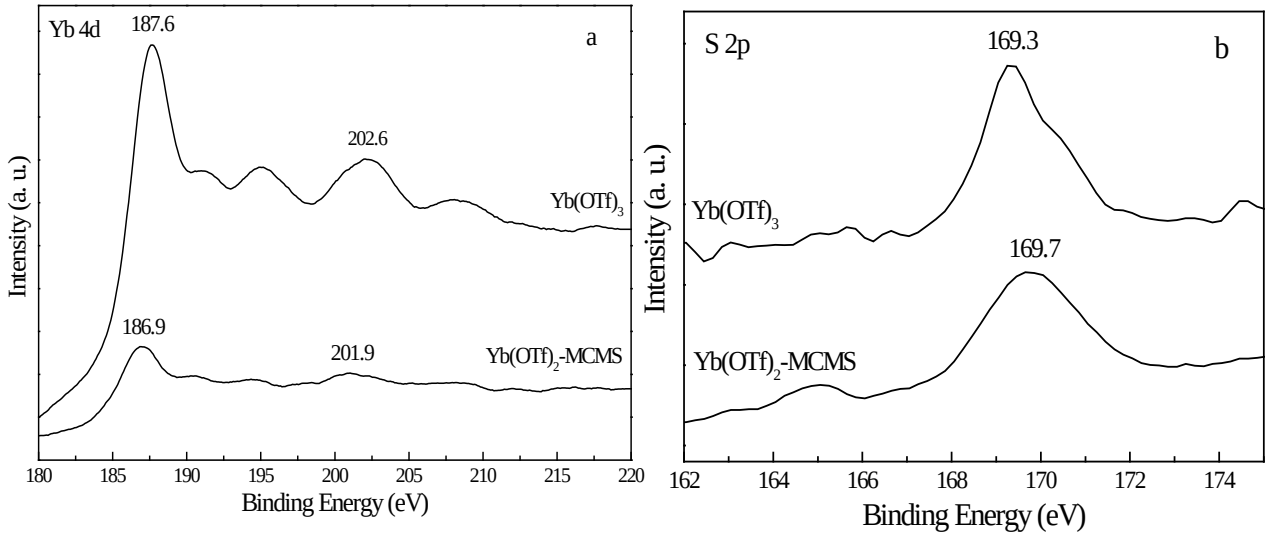

Figure 2 XPS spectra of $Yb(OTf)_2$-SO_3Na&Ph-MCMSS catalyst (a. Yb 4d; b. S 2p).

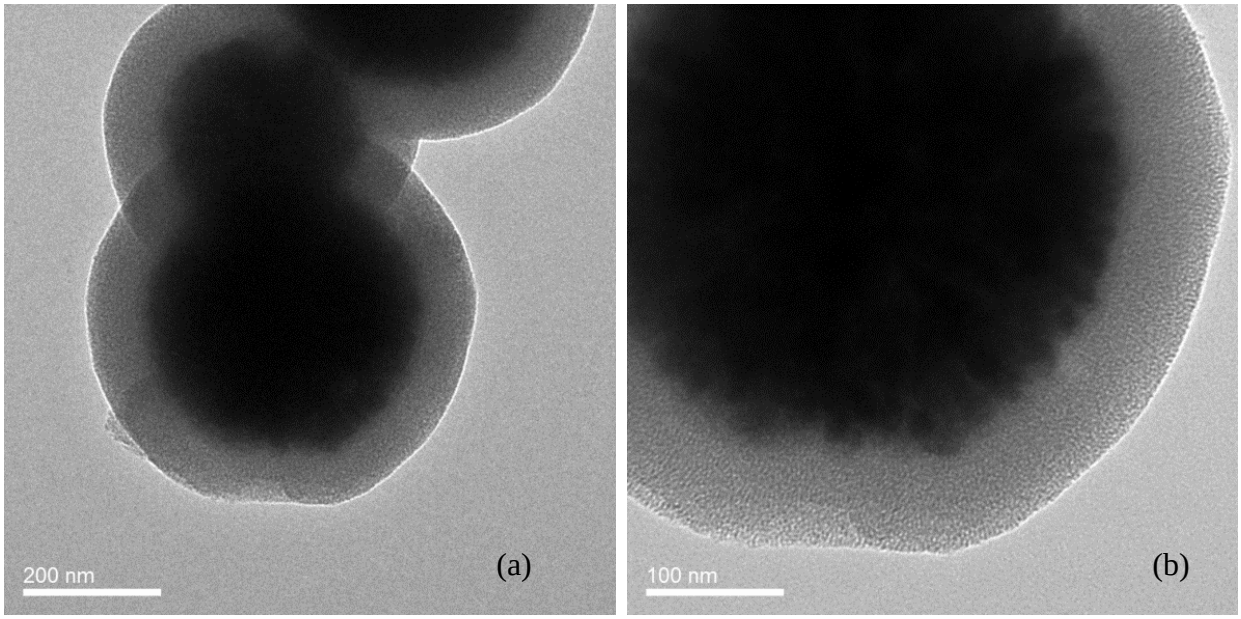

Figure 3 TEM pictures of $Yb(OTf)_2$-SO_3Na&Ph-MCMSS catalyst.

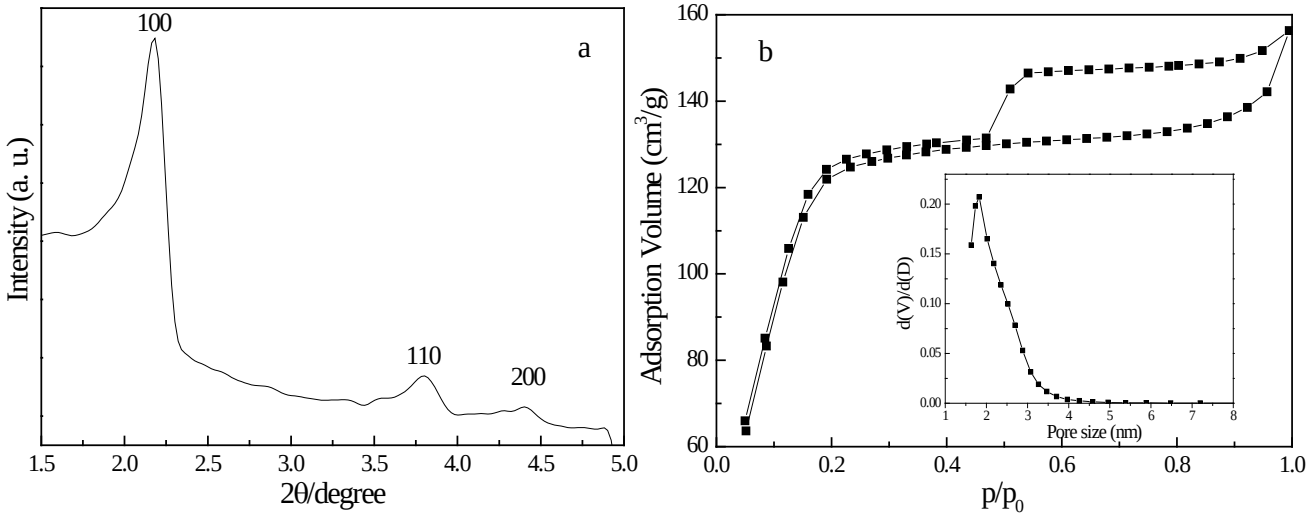

Figure 4 Low-angle XRD pattern (a), N_2 sorption curve (b) and pore size distribution (inset) of Yb(OTf)$_2$-SO$_3$Na&Ph-MCMSS catalyst.

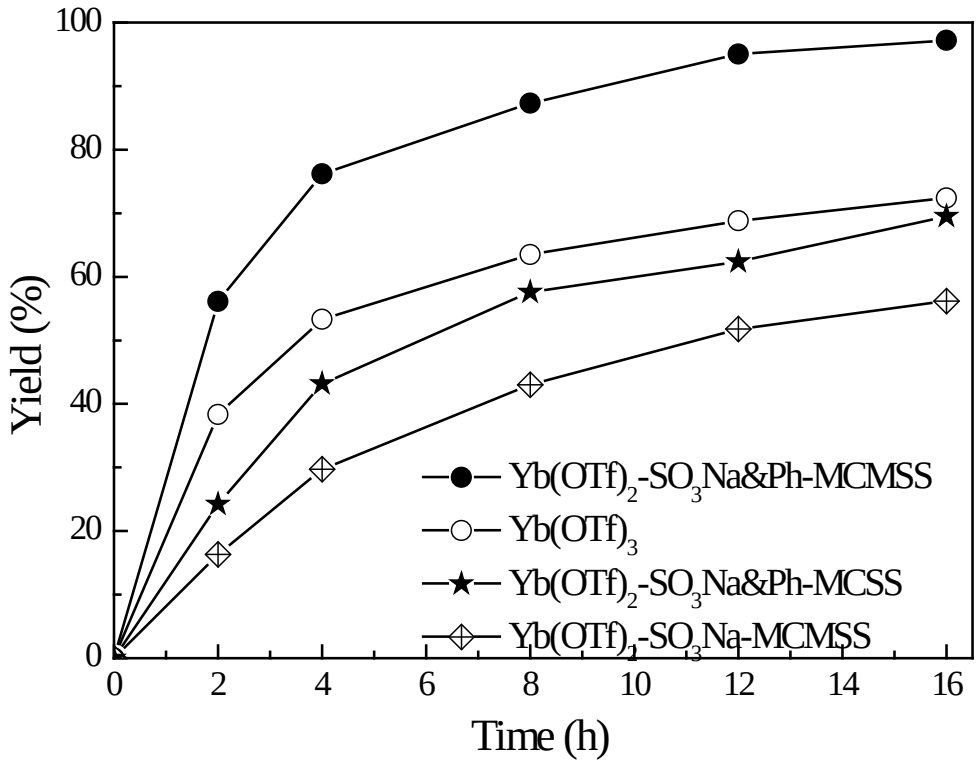

Figure 5 Reaction profiles over time in water-medium Mukaiyama-Aldol reaction between benzaldehyde and trimethyl(1-phenylprop-1-enyloxy)silane over different catalysts. Reaction conditions are given in Table 1.

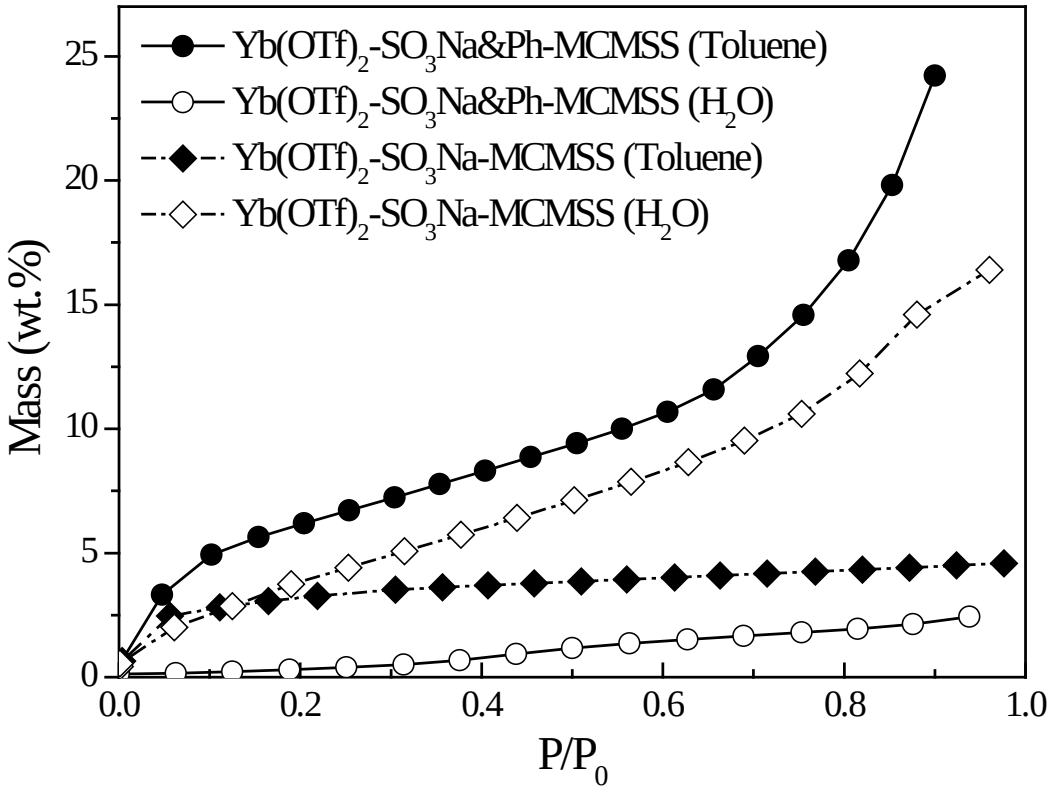

Figure 6 Hydrophobicity tests of $Yb(OTf)_2$-SO_3Na&Ph-MCMSS and $Yb(OTf)_2$-SO_3Na-MCMSS catalysts.

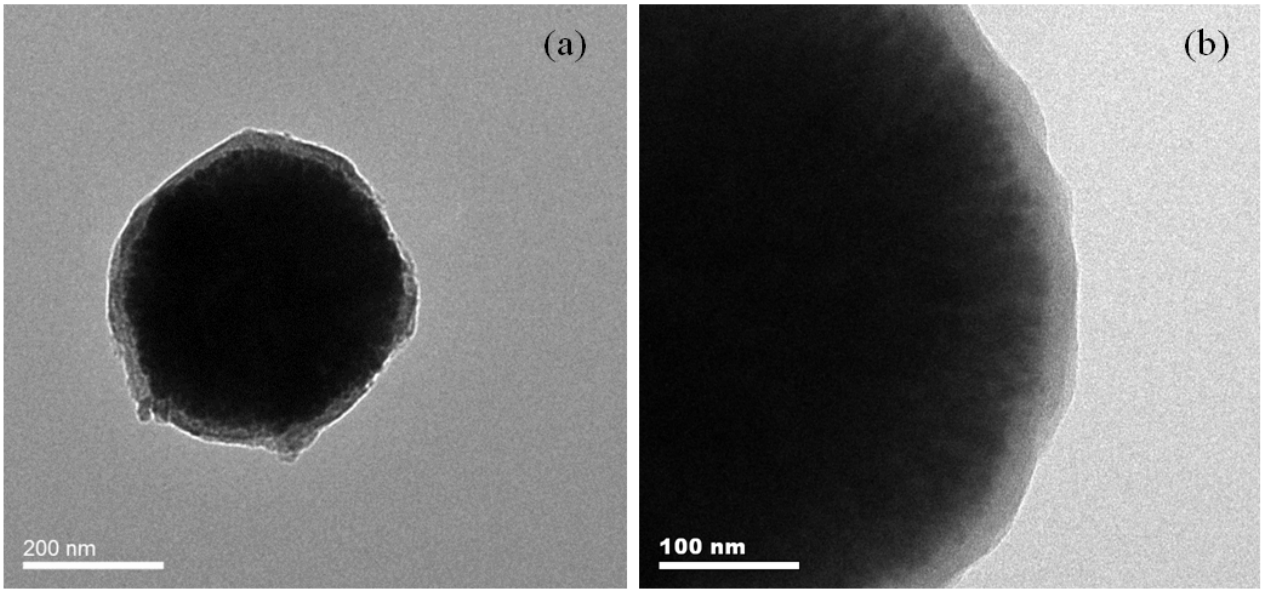

Figure 7 TEM images of $Yb(OTf)_2$-SO_3Na&Ph-MCSS catalyst.

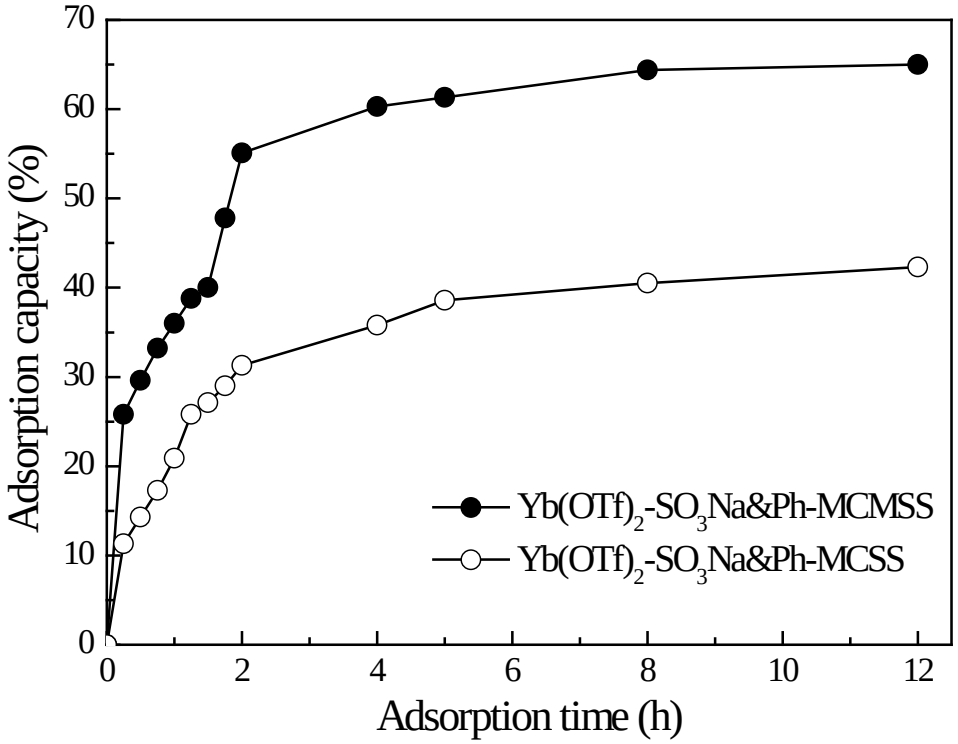

Figure 8 Benzaldehyde adsorption profiles over $Yb(OTf)_2$-SO_3Na&Ph-MCMSS and $Yb(OTf)_2$-SO_3Na&Ph-MCSS catalysts.

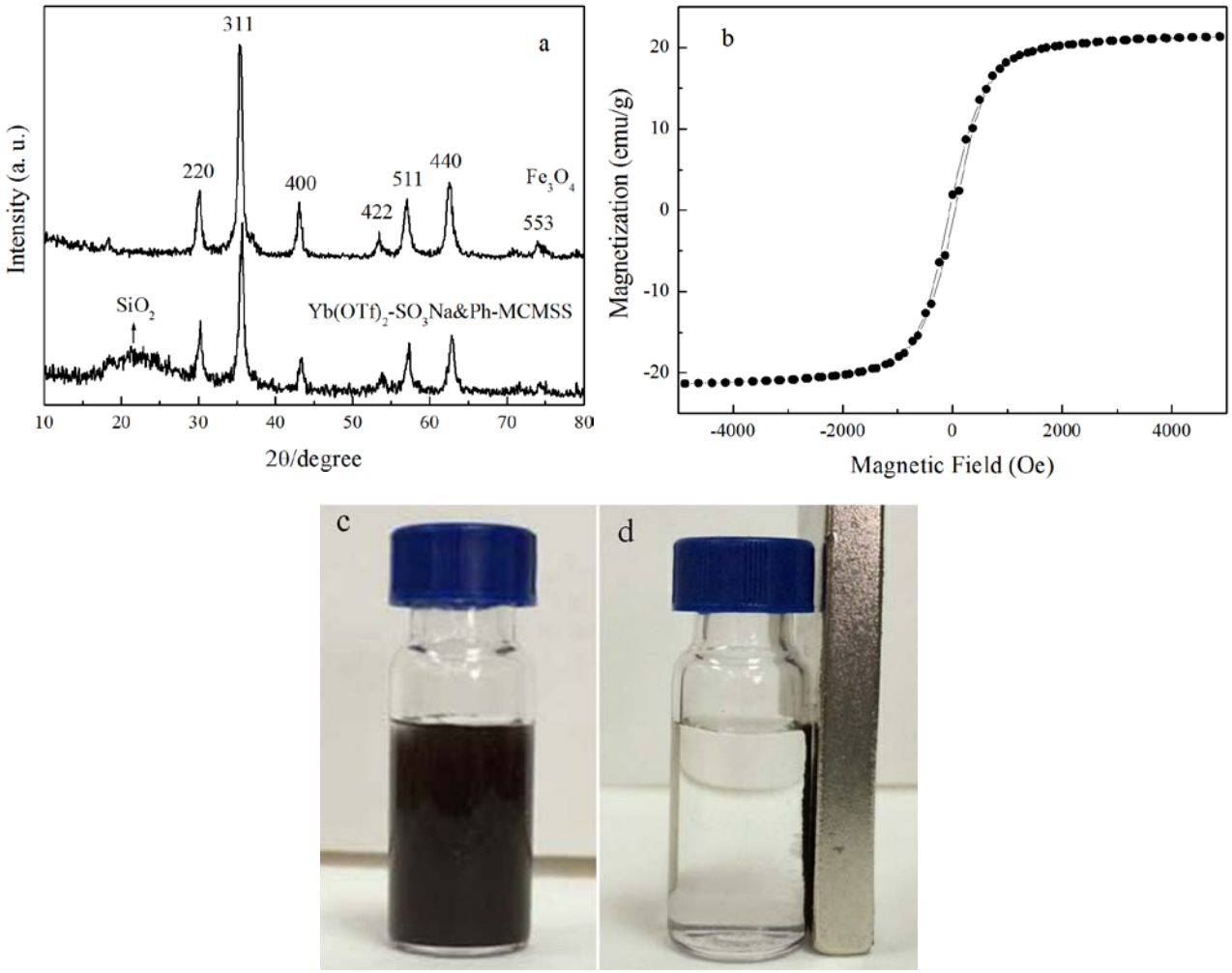

Figure 9 (a) Wide-angle XRD patterns of Fe_3O_4 and Yb(OTf)$_2$-SO$_3$Na&Ph-MCMSS samples, (b) Magnetization curve of the Yb(OTf)$_2$-SO$_3$Na&Ph-MCMSS catalyst determined at room temperature, (c) the reaction mixture containing the Yb(OTf)$_2$-SO$_3$Na&Ph-MCMSS catalyst, and (d) the reaction mixture containing the Yb(OTf)$_2$-SO$_3$Na&Ph-MCMSS catalyst with the application of a magnet.

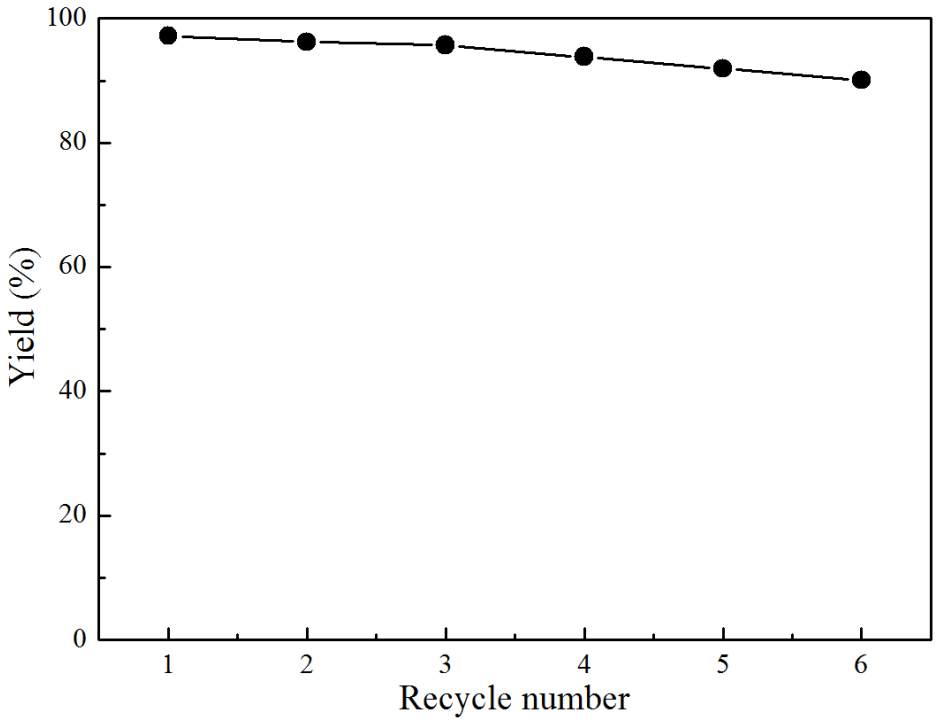

Figure 10 The recycling tests of $Yb(OTf)_2$-SO_3Na&Ph-MCMSS catalyst in water-medium Mukaiyama-Aldol reaction. Reaction condition was shown in Table 1.